Interaction of the Indole Class of Vacuolar H^+-ATPase Inhibitors with Lipid Bilayers†

F. Fernandes,‡ L. Loura,‡,§ R. B. M. Koehorst,|| N. Dixon,⊥ T. P. Kee,⊥ M. A. Hemminga,|| and M. Prieto*,‡

Centro de Química-Física Molecular, Instituto Superior Técnico, Lisbon, Portugal, Departamento de Química, Universidade de Évora, Évora, Portugal, Laboratory of Biophysics, Wageningen University, Wageningen, The Netherlands, and Department of Chemistry, University of Leeds, Leeds LS2 9JT, United Kingdom

Received November 7, 2005; Revised Manuscript Received March 8, 2006

ABSTRACT: The selective inhibitor of osteoclastic V-ATPase (2*Z*,4*E*)-5-(5,6-dichloro-2-indolyl)-2-methoxy-*N*-(1,2,2,6,6-pentamethylpiperidin-4-yl)-2,4-pentadienamide (SB 242784), member of the indole class of V-ATPase inhibitors, is expected to target the membrane-bound domain of the enzyme. A structural study of the interaction of this inhibitor with the lipidic environment is an essential step in the understanding of the mechanism of inhibition. In this work, a comprehensive study of the relevant features of this interaction was performed. Inhibitor partition coefficients to lipid vesicles as well as its transverse location, orientation (order parameters), and dynamics while bound to bilayers were determined through photophysical techniques, taking advantage of the intrinsic fluorescence of the molecule. To better evaluate the functionally relevant features of SB 242784, a second inhibitor, INH-1, from the same class and having a reduced activity was also examined. It is shown that regarding membrane interaction their properties remain very similar for both molecules, suggesting that the differences in inhibition efficiencies are solely a consequence of the molecular recognition processes within the inhibition site in the V-ATPase.

Bone degradation requires a lowering of pH in the resorption lacuna (extracellular space between the osteoclast cell and bone surface) (*1*). This is achieved through pumping of protons by V-ATPases[1] located in the ruffled border of osteoclasts (*2*). Inhibitors of osteoclast V-ATPase activity could therefore be used in new therapeutics for treatment of bone diseases related to excess bone resorption, namely, osteoporosis.

The macrolide antibiotic bafilomycin is a powerful inhibitor of V-ATPases (*3*) and was shown to prevent bone resorption (*4*). Nevertheless, due to the lack of specificity of bafilomycin toward osteoclastic V-ATPase, several other important V-ATPases are inhibited, and this is responsible for the extremely high toxicity and, consequently, for the clinical inadequacy of this compound. Recently, some derivatives of bafilomycin have been synthesized which maintained high inhibitory activity toward V-ATPases and exhibited high selectivity for the osteoclast form of the enzyme (*5*, *6*). The most promising of these compounds, (2*Z*,4*E*)-5-(5,6-dichloro-2-indolyl)-2-methoxy-*N*-(1,2,2,6,6-pentamethylpiperidin-4-yl)-2,4-pentadienamide (SB 242784) (Figure 1), was shown to have more than 1000-fold selectivity for the osteoclast V-ATPase compared with the enzyme measured in kidney, liver, spleen, stomach, brain, or endothelial cells and to have no effect on other cellular ATPases. SB 242784 was also extremely effective in preventing bone loss in ovariectomized rats (*7*). This inhibitor is therefore a promising candidate for osteoporosis treatment.

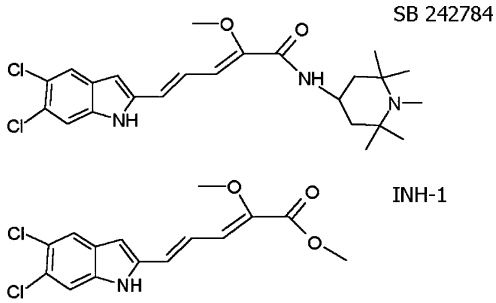

FIGURE 1: Chemical structures of SB 242784 and INH-1.

The site of action of bafilomycin in the enzyme was shown to be located in the membrane-bound domain (*8*−*11*). Therefore, the type and extent of the interaction of the bafilomycin derivative SB 242784 with the lipid environment and the properties of the inhibitor molecule while in this medium are relevant, since it is expected that the first step prior to the interaction with the enzyme is the membrane

† This work was supported by Contract QLG-CT-2000-01801 of the European Commission (MIVase Consortium) and by FCT (Portugal) under the Program POCTI. M.A.H. and M.P. are members of the COST D22 Action of the European Union. F.F. acknowledges Grant SFRH/BD/14282/2003 from FCT (Portugal).

* Corresponding author. E-mail: prieto@alfa.ist.utl.pt. Telephone: (+351) 218413248. Fax: (+351) 218464455.

‡ Instituto Superior Técnico.

§ Universidade de Évora.

|| Wageningen University.

⊥ University of Leeds.

[1] Abbreviations: V-ATPase, vacuolar H^+-ATPase; DOPC, 1,2-dioleoyl-*sn*-glycero-3-phosphocholine; DOPG, 1,2-dioleoyl-*sn*-glycero-3-[phospho-*rac*-(1-glycerol)]; DMPC, 1,2-dimyristoyl-*sn*-glycero-3-phosphocholine; 5-DOX-PC, 1-palmitoyl-2-stearoyl(5-DOXYL)-*sn*-glycero-3-phosphocholine; 12-DOX-PC, 1-palmitoyl-2-stearoyl(12-DOXYL)-*sn*-glycero-3-phosphocholine; SB 242784, (2*Z*,4*E*)-5-(5,6-dichloro-2-indolyl)-2-methoxy-*N*-(1,2,2,6,6-pentamethylpiperidin-4-yl)-2,4-pentadienamide, INH-1, methyl (2*Z*,4*E*)-5-(5,6-dichloro-2-indolyl)-2-methoxy-2,4-pentadienoate.

10.1021/bi0522753 CCC: $33.50
Published on Web 04/05/2006

incorporation of the inhibitor with the concomitant increase of its effective concentration.

Recently, spin-labeled derivatives of SB 242784 have been studied by electron spin resonance (ESR) (*12*). It was then possible to acquire information regarding the location in the membrane of the piperidine ring where the nitroxide label was inserted. However, a photophysical approach would enable a report on the whole molecule, since the indole ring is conjugated with the double bond system, and this is largely expected to dictate the inhibitor properties in the lipid phase.

In this work we report a thorough study on the interaction of SB 242784 with lipid vesicles together with a detailed study of the compound behavior in aqueous solution, using for this effect its intrinsic photophysical properties (absorption, fluorescence, fluorescence anisotropy, linear dichroism), thus avoiding the derivatization of the molecule. The water−lipid partition coefficient of SB 242784 was determined, and its aggregation was studied. The position and orientation of the molecule when interacting with lipid bilayers were also obtained. The same studies were performed with another less powerful inhibitor of the same class (INH-1) to compare the results and retrieve information on the relevance of specific structural features of SB 242784 on these properties.

MATERIALS AND METHODS

DOPC, DOPG, and DMPC were obtained from Avanti Polar Lipids (Birmingham, AL). 5-DOX-PC and 12-DOX-PC were from Avanti Polar Lipids (Birmingham, AL). Fine chemicals were obtained from Merck (Darmstadt, Germany). All materials were used without further purification.

SB 242784 and INH-1 were synthesized according to Nadler et al. (*6*) and Gagliardi et al. (*5*).

Inhibitor Incorporation in Lipid Vesicles. The V-ATPase inhibitors were incorporated in lipid vesicles by two different methods: In the cosolubilization method the phospholipid and inhibitor solutions were mixed in chloroform and dried under a flow of dry N_2. The last traces of solvent were removed under vacuum. Multilamellar vesicles were then obtained through solubilization in Tris buffer, and large unilamellar vesicles (LUVs) were produced by extrusion through polycarbonate filters with a pore size of 100 nm (*13*). In an alternative method of incorporation, a very small volume (<1% of total volume) of an ethanolic solution of the inhibitor was added to the already prepared LUVs and immediately mixed. Except for the comparison of partition coefficients, the first method was always used.

The phospholipid concentration in the samples was determined through quantification of inorganic phosphate according to McClare (*14*). The lipid to inhibitor ratio was always kept above 250 except for linear dichroism measurements when it was 30.

Preparation of Aligned DMPC/SB 242784 and DMPC/INH-1 Multilayers for Linear Dichroism Measurements. Multilamellar vesicles with incorporated inhibitors were prepared as described above using Millipore water. A small volume (30 μL) of the suspension was spread on the surface of a quartz plate, and the water was slowly evaporated under a mild stream of dry N_2 as described in Castanho et al. (*15*).

Absorption and Fluorescence Spectroscopy. Absorption spectroscopy was carried out with a Jasco V-560 spectrophotometer (Tokyo, Japan). The absorption of the samples was kept below 0.1 at the wavelength used for excitation.

Steady-state fluorescence measurements were carried out with an SLM-Aminco 8100 series 2 spectrofluorometer (Rochester, NY; with double excitation and emission monochromators, MC400) in a right angle geometry. The light source was a 450 W Xe arc lamp, and for reference a Rhodamine B quantum counter solution was used. Quartz cuvettes (1 × 1 cm) were used. All measurements were performed at room temperature.

Steady-state anisotropies were determined according to the equation (*16*)

$$\langle r \rangle = \frac{I_{VV} - GI_{VH}}{I_{VV} + 2GI_{VH}} \quad (1)$$

where the different intensities I_{ij} are the steady-state vertical and horizontal components of the fluorescence emission with excitation vertical (I_{VV} and I_{VH}, respectively) and horizontal (I_{HV} and I_{HH}, respectively) to the emission axis. The latter pair of components is used to calculate the G factor ($G = I_{HV}/I_{HH}$) (*17*). Polarization of excitation and emission light was achieved using Glan-Thompson polarizers. SB 242784 anisotropies were recorded with excitation and emission wavelengths of 365 and 436 nm, respectively, with spectral bandwidths of 4 nm. For INH-1 the same bandwidth was kept, but the emission wavelength was 462 nm. For SB 242784 in water, fluorescence emission intensities were measured at 505 nm as this corresponds to the maximum of the spectrum in water. For the same reasons, the wavelengths taken for INH-1 measurements in these solvents were 367 and 511 nm.

SB 242784 and INH-1 quantum yields were determined using quinine bisulfate dissolved in 1 N H_2SO_4 [$\phi = 0.55$ (*18*)] as a reference.

Fluorescence decay measurements of the inhibitors were carried out with a single-photon timing system, which is described elsewhere (*19*). Measurements were performed at room temperature, with excitation and emission wavelengths of 360 and 435 nm, respectively. Data analysis was carried out using a nonlinear, least-squares iterative convolution method based on the Marquardt algorithm (*20*). The goodness of the fit was judged from the experimental χ^2 value, weighted residuals, and autocorrelation plot.

In all cases, the probe florescence decay was complex and described by a sum of exponentials:

$$I(t) = \sum_i a_i \exp(-t/\tau_i) \quad (2)$$

where a_i are the normalized amplitudes and τ_i are the fluorescence lifetimes.

For the linear dichroism measurements, the quartz plate covered with aligned multilayers was positioned in a goniometer (Optosigma, SL), which replaced the standard cell holders of both the spectrophotometer and the spectrofluorometer, and dichroic ratios were measured in the range of 0−72° and 18−72°, respectively.

The order parameters ($\langle P_2 \rangle$ and $\langle P_4 \rangle$) are obtained from the equations:

$$\frac{\sin(\omega)A_\omega}{A_{\omega=(\pi/2)}} = 1 + \frac{3\langle P_2 \rangle}{(1 - \langle P_2 \rangle)n^2}\cos^2 \omega \quad (3)$$

$$I_{VH}/I_{VV} = a \sin^2 \alpha + b \quad (4)$$

A_ω is the absorbance at angle ω, n is the refraction index [$n = 1.5$ (*21*)], α is the angle at which the fluorescence is measured, and the a and b parameters depend on both $\langle P_2 \rangle$ and $\langle P_4 \rangle$. Complete formalisms and further details are described in Lopes et al. (*22*).

Dichroic ratios were determined using Glan-Thompson polarizers. In fluorescence emission measurements for determination of $\langle P_4 \rangle$, excitation and emission wavelengths were kept the same as in the remaining steady-state measurements.

From the knowledge of $\langle P_2 \rangle$ and $\langle P_4 \rangle$, a combination of the maximum entropy method together with the formalism of the Lagrange multipliers is used to describe the single particle distribution function $f(\Psi)$, where Ψ is the angle between the transition moment of the molecule and the director of the system (normal to the bilayer plane). This distribution is the broadest one that is compatible with the experimental order parameters, and to obtain the population density probability function, which is the probability of finding the transition moment between Ψ and $\Psi + d\Psi$, it should be multiplied by sin Ψ (*22*).

The determination of the transition moment of SB 242784 was performed for an optimized geometry of the molecule based on the *d*ensity *f*unctional *t*heory (DFT) (*23*), which recovered the 2*Z*,4*E* isomer that is the preponderant species (*6*). The theoretical level applied to the calculations was Becke3LYP/6-31G(d) (*24*−*26*).

RESULTS

Indole Inhibitor Behavior in Aqueous Environment. Since the interaction with the membrane proceeds from the inhibitors in aqueous solution, their characterization in an aqueous environment was first carried out. Preliminary results showed both SB 242784 and INH-1 (Figure 1) to be unstable under aqueous condition (*27*). The fluorescence quantum yield of the two molecules in aqueous buffer was extremely low (0.01 and 0.004 for SB 242784 and INH-1, respectively) when compared with the quantum yield observed in other environments (e.g., 0.06 and 0.05 for SB 242784 and INH-1 in ethanol, respectively). The large decrease in fluorescence intensity of the inhibitors is the result of formation of nonfluorescent or "dark" aggregates, as the quantum yield values determined from transient state fluorescence measurements were larger than the ones obtained from steady-state data. This aggregation is due to the hydrophobic character of the inhibitors, and the fluorescence quenching effect is enhanced by the presence of chlorine atoms in the molecule. In the present work we measured the extent and kinetics of aggregation of both inhibitors in an aqueous environment. For this purpose, fluorescence intensity measurements were started immediately after addition of 10 μL of a ethanol stock solution to a cuvette containing 3 mL of buffer under permanent stirring, and the final concentration of inhibitor in buffer was 4 μM. The buffer used was 10 mM Tris and 150 mM NaCl, pH 7.4. The result for SB 242784 is presented in Figure 2. The kinetics for the aggregation in water of INH-1 was very fast, and the phenomenon could not be resolved as well as it was for SB 242784. In addition, the extent of aggregation, as taken from the remaining fluorescence intensity after the process reaches equilibrium, was larger for INH-1 than for SB 242784. For both inhibitors the fluorescence intensity increased dramatically upon addition of sodium dodecyl sulfate to the samples (results not shown), this suggesting disruption of aggregates and emission of monomeric inhibitors dispersed in the micellar medium and ruling out a significant contribution of photobleaching.

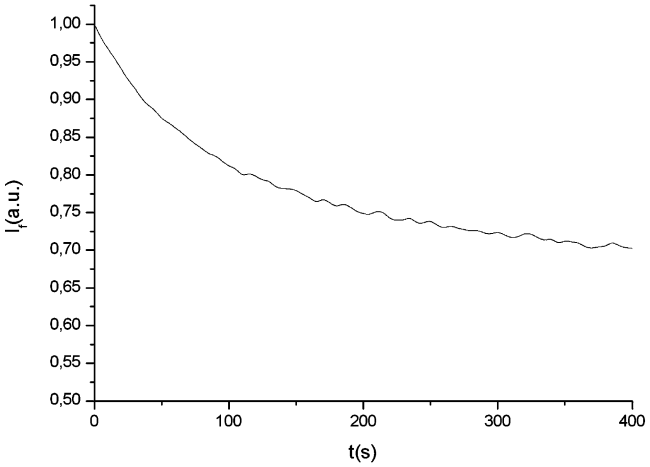

FIGURE 2: SB 242784 fluorescence emission self-quenching induced by aggregation in an aqueous environment. The buffer used was 10 mM Tris and 150 mM NaCl, pH = 7.4.

The anisotropies of INH-1 and SB 242784 in water were 0.20 and 0.22, respectively, and did not change during the process of aggregation. This indicates that the aggregates being formed are nonfluorescent, and the residual emission of monomeric species is the one contributing to anisotropy.

In an attempt to determine the existence of a critical micellar concentration (cmc) for the inhibitors in an aqueous environment, we measured fluorescence emission intensities for inhibitor solutions with concentrations up to 4 μM. A cmc should appear as a change in linearity of fluorescence intensity vs inhibitor concentration. However, a completely linear plot was obtained up to 10 nM, the limit of detection of the fluorometer (results not shown). Therefore, the aggregation offset, if existing at all, should occur for both inhibitors in water at concentrations below 10 nM, and therefore no evidence was obtained for micellar-type aggregates of these inhibitors.

Inhibitor Partition to Lipid Vesicles. The fluorescence emission spectra of SB 242784 and INH-1 in the presence of DOPC vesicles are presented in Figure 3. DOPC and DOPG lipids were chosen for the reconstitution of the inhibitors because SB242784 was used by us in binding assays to selected transmembrane peptide fragments of V-ATPase that required DOPC (and in some cases a small fraction of DOPG) for correct peptide conformation while inserted in liposomes (unpublished experiments). Using the cosolubilization method for incorporation of the inhibitors (see Materials and Methods section), the fluorescence emission maximum for SB 242784 is 436 nm whereas for INH-1 it is 461 nm. On the other hand, in DOPC−DOPG (80:20 mol/mol) bilayers, the SB 242784 fluorescence

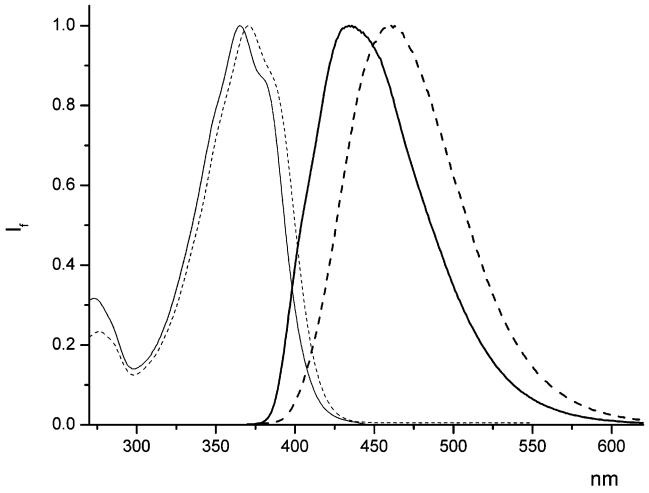

FIGURE 3: Absorption and fluorescence emission spectra of the indole class of V-ATPase inhibitors. Fluorescence emission spectra were obtained using excitation wavelengths corresponding to the maxima of each inhibitor: (thin dashed line) absorption spectrum of INH-1; (thin solid line) absorption spectrum of SB 242784; (thick dashed line) fluorescence spectrum of INH-1; (thick solid line) fluorescence spectrum of SB 242784.

emission maximum was 432 nm. For the alternative incorporation method of adding the inhibitor to the preformed vesicles, the fluorescence emission maxima were slightly blue shifted (≈3 nm) when comparing with the previous values, but after a small period of time (≈5 min) they became identical to the ones obtained through the cosolubilization method, thus suggesting that the initially formed aggregates are disrupted upon membrane interaction. The quantum yields of SB 242784 and INH-1 determined in the presence of 2 mM DOPC LUVs were 0.15 and 0.10, respectively. These values are not biased by the fraction of inhibitors in the aqueous phase, because at this lipidic concentration it can be concluded from the determined partition coefficients (see below) that the inhibitors are almost completely incorporated in the membrane (>95%), and in addition, the quantum yield in water is negligible.

Although an extremely large blue shift in the inhibitor fluorescence is observed upon incorporation in lipid vesicles (e.g., the maximum emission wavelength of SB 242784 in water is 505 nm), this is not per se evidence for a large extent of partitioning of the two molecules to the lipid environment, because, as mentioned above, the quantum yield in the aqueous medium is very low due to aggregation. To obtain a quantitative description, both the extent and kinetics of the partition of both inhibitors to DOPC vesicles were studied. Partition coefficients were determined through monitoring of the change in fluorescence emission intensity (I) vs lipid concentration [L] (Figure 4) and applying the equation (*28*):

$$I = \frac{I_w + K_p \gamma_L [L] I_L}{1 + K_p \gamma_L [L]} \quad (5)$$

where I_w is the fluorescence of the fluorophore in water, I_L is the fluorescence of the fluorophore incorporated in the lipid vesicles, K_p is the partition coefficient defined in terms of solute concentrations in each phase, and γ_L is the lipid molar volume [0.78 dm^{-3} mol^{-1} for DOPC (*29*)]. The results

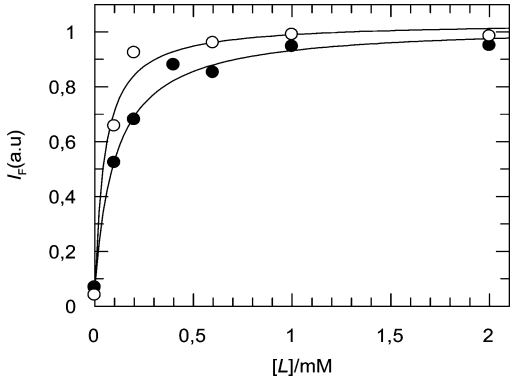

FIGURE 4: Increase in steady-state fluorescence emission intensity of indole V-ATPase inhibitors with lipid concentration: (●) SB 242784 incorporated in DOPC vesicles by the cosolubilization method; (○) INH-1 incorporated in DOPC vesicles by the method of addition after lipid solubilization. The buffer used was 10 mM Tris and 150 mM NaCl, pH = 7.4. The lines represent the fits of eq 5 to the data, and the partition coefficients are shown in Table 1.

Table 1: V-ATPase Inhibitor Partition Coefficients to Lipid Vesicles

	system		
inhibitor	cosolubilization with DOPC	cosolubilization with DOPC−DOPG	addition to liposomes with DOPC
SB 242784	$(1.20 \pm 0.08) \times 10^4$	$(6.64 \pm 1.76) \times 10^3$	$(1.29 \pm 0.23) \times 10^4$
INH-1	$(1.49 \pm 0.26) \times 10^4$		$(2.84 \pm 0.99) \times 10^4$

from a nonlinear fitting of eq 5 to the experimental data are shown in Table 1.

For SB 242784, the anisotropy obtained while adding the inhibitor to preformed vesicles was $\langle r \rangle = 0.33$, the same value being obtained through the cosolubilization method. In vesicles composed of DOPC−DOPG (4:1 mol/mol), SB 242784 anisotropy was virtually identical ($\langle r \rangle = 0.32$). The INH-1 anisotropy in samples with preformed vesicles ($\langle r \rangle = 0.24$) was lower than observed for the same molecule incorporated by cosolubilization ($\langle r \rangle = 0.31$). Again, these experiments were carried out at a lipidic concentration for which the fraction of light emitted from inhibitor molecules in water is negligible.

Inhibitor Transverse Location in Lipid Vesicles. The effects on the inhibitors' fluorescence emission spectral shape and intensity caused by the presence of nitroxide-labeled lipid in DOPC vesicles were investigated. A 10% ratio of labeled (5- or 12-DOX-PC) to nonlabeled lipids was used. For SB 242784, there was a very slight shift on the fluorescence emission maximum, depending on the nitroxide-labeled lipid present. In the absence of quenchers the fluorescence emission maximum was at 436 nm, whereas in the presence of 5-DOX-PC this wavelength was 435 nm. Using 12-DOX-PC a red shift was obtained, the maximum being now 438 nm (Figure 5A). For INH-1, there was no difference in the shape of the emission spectrum in the presence of 12-DOX-PC (maxima were at 461 nm), but using 5-DOX-PC a very small blue shift (2 nm) was obtained (Figure 5B). These shifts are evidence that the two nitroxide labels, which are localized at different depths in the membrane, are selectively quenching inhibitor populations which lie at different transverse positions.

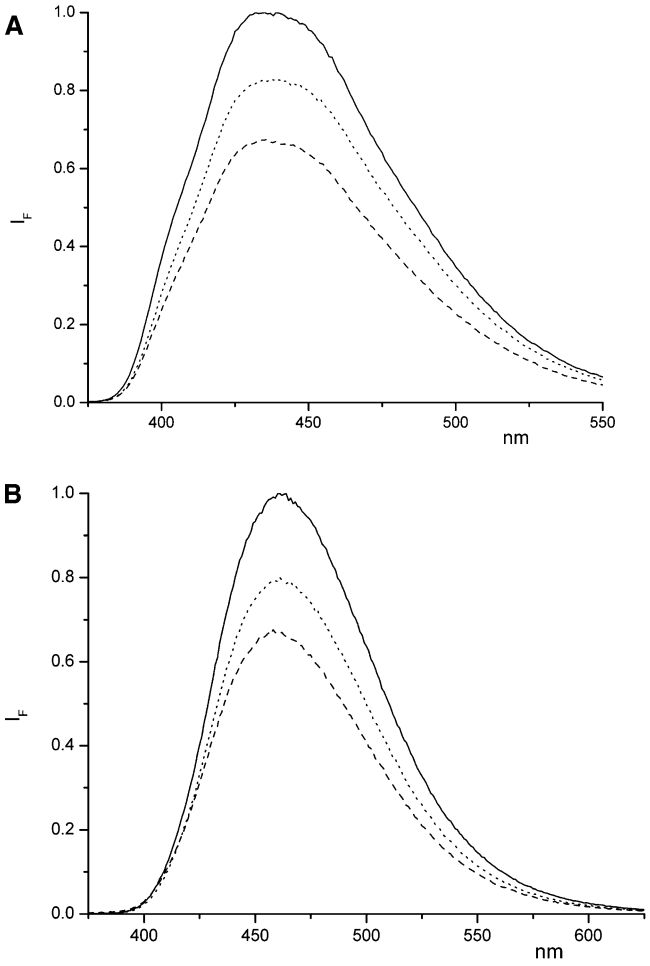

FIGURE 5: Fluorescence emission spectra of indole V-ATPase inhibitors in the absence (—) and presence of different nitroxide-labeled lipids: (- - -) 5-DOX-PC and (•••) 12-DOX-PC). (A) SB 242784. (B) INH-1.

Quantitative information on the inhibitor location in the membrane can be obtained via the so-called parallax method (*30*) using the equation:

$$z_{cf} = L_{cl} + (-\ln(F_1/F_2)/\pi C - L_{21}^2)/2L_{21} \qquad (6)$$

where z_{cf} is the distance of the fluorophore from the center of the bilayer, F_1 is the fluorescence intensity in the presence of the surface-located quencher (5-DOX-PC), F_2 is the fluorescence intensity in the presence of the quencher located deeper in the membrane (12-DOX-PC), L_{c1} is the distance of the shallow quencher from the center of the bilayer, L_{c2} is the distance of the deep quencher from the center of the bilayer, L_{21} is the distance between the shallow and deep quenchers ($L_{c1} - L_{c2}$), and C is the concentration of the quencher in molecules/Å^2. Using the distances of the nitroxide quenchers from the center of the bilayer given by Abrams and London (*31*), the obtained position for INH-1 was of 11.9 Å from the center of the bilayer, whereas for SB 242784 this value was 12.8 Å.

To gain further information regarding the inhibitors' location in the membrane, acrylamide quenching assays were also performed. Acrylamide is a hydrophilic quencher, and therefore differences in the extent of quenching by acrylamide allow a direct comparison of the bilayer penetration by the fluorophores. Acrylamide quenched both inhibitors with very similar efficiencies (results not shown), and a very slightly increased quenching observed for INH-1 is due to the also slight difference in average lifetimes (*16*) for the two inhibitors while incorporated in DOPC vesicles ($\langle\tau\rangle_{INH-1} = 0.60$ ns and $\langle\tau\rangle_{SB\ 242784} = 0.55$ ns), because the Stern−Volmer rate constant is the product between the effective bimolecular rate constant (which can be decreased due to fluorophore shielding from the quencher) and the intrinsic lifetime of the fluorophore.

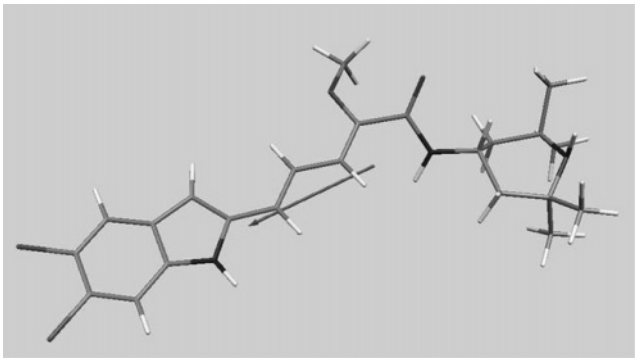

FIGURE 6: Orientation of the transition moment of SB 242784, obtained from TD-DFT calculations (see text for details).

Table 2: Order Parameters and Lagrange Coefficients of the Two Inhibitors in DOPC Multilayers Obtained from Linear Dichroism Studies[a]

	$\langle P_2\rangle$	$\langle P_4\rangle$	λ_2	λ_4
SB 242784	0.15	−0.21	0.99	−2.31
INH-1	0.18	−0.31	1.27	−4.67

[a] See text for details.

Inhibitor Orientation in Lipid Vesicles. From the linear dichroism methodology, information regarding the orientation of the transition moment is obtained. In this way, to obtain information about the orientation of the molecule regarding the director of the system (normal to the membrane interface), it is necessary to know the orientation of the transition moment relative to the molecular axes. To this effect, a quantum chemical calculation was carried out.

Applying *t*ime-*d*ependent *d*ensity *f*unctional *t*heory (TD-DFT) to an energy-optimized geometry of SB 242784, the orientation of the transition dipole moment relative to the molecule structure was obtained. As shown in Figure 6, the transition dipole moment is almost parallel to the molecular axis defined by the double bond conjugated system, and an approximately identical transition dipole moment orientation can be considered for INH-1, as both molecules have very similar fluorophores and the molecular differences are not expected to largely influence this property.

The orientation parameters $\langle P_2\rangle$ and $\langle P_4\rangle$ and Lagrange coefficients obtained for INH-1 and SB 242784 from the linear dichroism measurements are presented in Table 2. The corresponding orientational density probability functions are shown in Figure 7.

DISCUSSION

Inhibitor Aggregation and Partition to Lipid Vesicles. It is surprising that INH-1 appears to aggregate in aqueous solution more readily and to a larger extent than SB 242784. The presence of the piperidine ring in the latter was expected

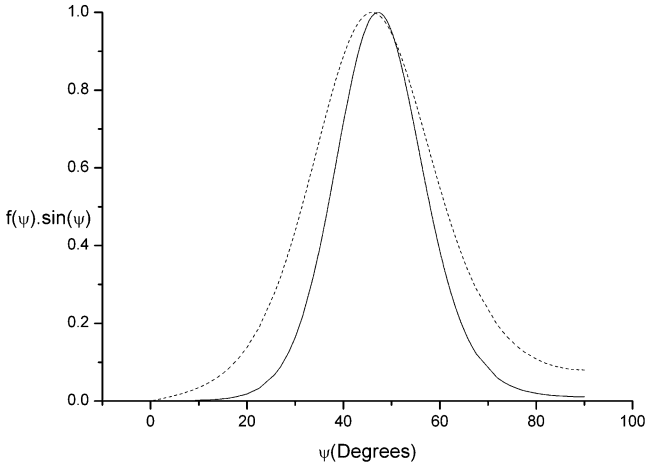

FIGURE 7: Orientation distribution function in DMPC of SB 242784 (- - -) and INH-1 (—).

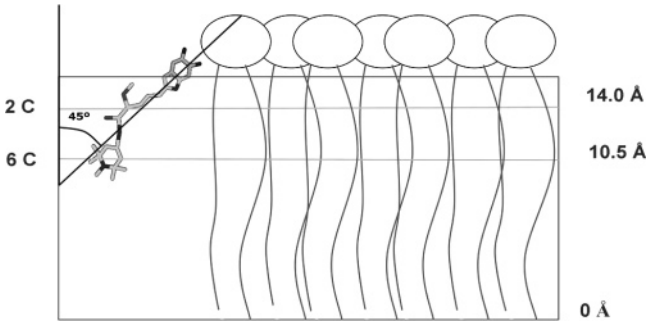

FIGURE 8: Proposed topography and orientation of SB 242784 in a DOPC bilayer. The molecule is depicted from the estimated most probable angle and depth (see Discussion).

to result in a smaller hydrophilicity, but this does not seem to be the case. Regarding the extent of aggregation, one possibility is that the piperidine ring induces a different type of packing in SB 242784 aggregates which quenches the molecule fluorescence less efficiently than in INH-1 aggregates, resulting in partially fluorescent aggregates. For INH-1 aggregates it is reasonable to assume that these would consist of stacked molecules with $\pi-\pi$ interactions, but for SB 242784, this type of $\pi-\pi$ stacking would not be able to exclude the piperidine ring from the aqueous environment and another aggregation geometry would have to come into play. The larger self-quenching of INH-1 in water would then not be solely dictated by the extent of aggregation but also related to a more effective geometry of packing regarding the quenching of fluorescence. The absence of a micellar type of aggregate for these inhibitors is most probably related to the absence of significative amphiphilic character.

Both inhibitors partition with a high efficiency to lipid vesicles, and for SB 242784 the partition coefficient is independent of the method of incorporation (Table 1). Nevertheless, the partition to the lipid phase is only complete at moderately high lipid concentrations (for a $K_p \approx 12000$, 95% of the total inhibitor population is incorporated only at a lipid concentration of 2 mM).

For INH-1, the molecule partitions slightly more effectively when added to the preformed liposomes, but the differences in the partition coefficients are close to the uncertainty of the measurements. On thermodynamic grounds the two partition coefficients should in fact be identical upon reaching equilibrium. However, in most situations, the one from cosolubilization is higher than adding the solute from the aqueous solution, this being the case among other situations when stable aggregates (e.g., micelles) are formed in water. The identical values observed for the two methodologies of incorporation are consistent with the absence of a cmc previously described. The lower value for the partition coefficient of SB 242784 in DOPC−DOPG bilayers indicates a decreased partition to the bilayer upon the change in headgroup composition. This effect will be addressed in detail below when the fluorescence emission shifts of the inhibitors are discussed.

INH-1 anisotropy was smaller when it was added to preformed vesicles ($\langle r \rangle = 0.24$) when compared with the one observed for the same molecule incorporated via cosolubilization ($\langle r \rangle = 0.31$), and this is likely to be related to energy migration inside aggregates in the membrane. As there is an overlap between the absorption and fluorescence emission spectra of the inhibitors (Figure 3), energy migration (energy homotransfer) is operative for two molecules of inhibitor lying in close proximity as in the case of an aggregate. The INH-1 Förster radius (R_0) (*16*) for energy migration while in lipid membranes is 11 Å (result not shown), and therefore for INH-1 in close proximity fluorescence depolarization is expected. The effects of energy migration can only be observed via the fluorescence anisotropy which is expected to decrease, since the fluorescence lifetime remains constant in this type of photophysical interaction. At variance with the aggregates in water, these aggregates must be fluorescent; i.e., there is no self-quenching, as in order to change the steady-state anisotropy they have to contribute to a significant fraction of the total fluorescence. This feature is probably related to the specific geometry of the aggregate in the membrane. In addition, in the case that quantitative dimer formation is invoked, the intermolecular distance would be 12.7 Å as concluded from the theoretical formalism (*32*); this is slightly larger than the distance for a collisional complex, so this would mean that no contact (static) fluorescence quenching would happen. Possibly, INH-1, when added to preformed vesicles, either (i) segregates to a membrane-perturbed region, and what is being observed is not strictly aggregate formation but increased probability of insertion in a membrane-perturbed area, leading to a higher local monomer concentration, such as observed for micelles (*33*) and membranes (*34*), or (ii) is only partially aggregated (with intermolecular distance <12.7 Å), and the observed anisotropy is an average of those of monomers and these strongly depolarized species. Another explanation would rely on considering a different membrane location, implying a different rotational dynamics for INH-1 and, so, a different anisotropy. However, this is not likely to happen because the spectral profiles are identical for both incorporation methods. This anisotropy value did not change after overnight incubation, demonstrating that there is no fast redistribution of the membrane locally enriched/aggregated INH-1. For this reason, to obtain an uniform distribution of inhibitors in the bilayer, it is likely necessary to use the cosolubilization method. This partial partition of INH-1 to lipid vesicles in an aggregated form can explain the slightly larger value of the partition coefficient of this molecule when it was added to preformed liposomes. For SB 242784 no such behavior was observed, and this stems from the

structural differences of the two molecules (presence of the piperididine ring in SB 242784).

Inhibitor Transverse Location and Orientation in Lipid Vesicles. The large blue shifts observed upon the incorporation of the inhibitors in lipid vesicles are an indication that the inhibitors are not adsorbed to the surface of the bilayer but are somehow buried, having some contact with the acyl chain region. The wavelengths of maximum fluorescence emission for both inhibitors (436 and 461 nm) are almost the same as the ones observed for the same molecules in acetone (*27*). Taking as a reference the dielectric constant of acetone ($\epsilon = 20.7$), the corresponding region of PC bilayers with the same polarity properties lies in the headgroup region, outside the hydrocarbon core of the bilayer (*35*, *36*), which for DOPC can be roughly located at >14 Å from the center of the bilayer (*29*). On the other hand, SB 242784 in solution only exhibited such a blue-shifted emission when solubilized in nonprotic solvents, and as such this inhibitor is likely not to be in contact with a high density of water molecules when in lipid bilayers, excluding the possibility of a strictly superficial position, and therefore a positioning in the polar/apolar interface of the bilayer is more likely. Although other factors such as hydrogen bonding might affect the emission properties of the fluorophores, it is worthwhile noting that in addition to both inhibitors having fluorescence properties almost identical to those observed in acetone, they are located almost at the same distance to the center of the bilayer, as observed by acrylamide quenching and the parallax method, the latter positioning SB 242784 and INH-1 at 12.8 and 11.9 Å from the center of the bilayer (corresponding approximately to the position of the fourth to third carbon of the DOPC acyl chain in the fluid state), respectively. The difference in the position between the two inhibitors is <1 Å and can be considered to lie within the uncertainty of the parallax method. The small disagreement when comparing the position obtained by the parallax method with the above-mentioned indications from the wavelength of maximum emission of the inhibitors can be ascribed to the size of the fluorophore moiety which is expected to span several angstroms across the bilayer. The orientation of the molecules determined by us through linear dichroism is far from parallel to the membrane surface (see below), and for a 45° orientation relative to the bilayer normal, the *trans*−*trans* isomers of the fluorophores are expected to span more than 4 Å in that direction. Additionally, both the anisotropy and the wavelength of maximum fluorescence emission of SB 242784 in the presence of a 20% fraction of DOPG become somewhat lower than in pure DOPC, reflecting a change in inhibitor environment when the composition of the headgroup region changes. This is a further evidence that the inhibitor is located near the interface of the bilayer. The large fluorescence emission maximum blue shift (4 nm) observed in the presence of PG lipids appears to indicate a somewhat deeper position in the lipid bilayer for the inhibitor, as the polarity of the headgroup region is expected to increase and as such, a red-shifted emission would be expected for an identical inhibitor position. However, this wavelength of maximum emission (432 nm) is still far from the wavelength of maximum emission observed for SB 242784 in diethyl ether (425 nm), which possesses a dielectric constant similar to the hydrocarbon core of the bilayer, and as such although slightly more buried, the inhibitor is still not completely inserted in the hydrophobic core of the bilayer. This alteration of the inhibitor lateral position in the presence of PG lipids might explain the smaller partition coefficient of SB 242784 obtained in the DOPC−DOPG mixture, as compared to pure DOPC vesicles. It should be stressed that there is no phase separation in this mixture, which otherwise could affect the partition coefficient (*37*).

It is therefore clear that the inhibitors' fluorophores reside in contact with the headgroup region. It is known that indole moieties have a large preference for the complex electrostatic environment of the headgroup section of the bilayer, especially near the carbonyl region (*38*, *39*). This preference is expected to originate from the indole aromaticity and to an exclusion of the flat rigid shape of the indole from the hydrocarbon core due to entropic reasons (*38*). In the indole class of V-ATPase inhibitors all these characteristics are maintained, and a strong anchoring in that region by the indole group could be expected. However, taking into account the results from the parallax measurements, which positioned the fluorophore in contact with the first carbons of the DOPC acyl chains, it is necessary to assume that the molecules penetrate to some extent into the hydrocarbon core. This insertion is probably performed through the conjugated double bonds in order to maintain the indole moiety in contact the headgroup region and allowing the hydrophobic conjugated double bonds and piperidine ring to position in the apolar environment of the acyl chains, as recently observed by ESR measurements with a spin labeled derivative of SB 242784 (*12*). In that study it was concluded that the nitroxide group connected to the piperidine ring in a DOPC bilayer lies at a depth corresponding to the location of the fifth carbon of the acyl chain, around 11 Å from the center of the bilayer. The value obtained here from the parallax method (12.8 Å) is compatible with this result, because our methodology positions the whole fluorophore and not solely the terminal piperidine ring.

The fluorescence anisotropies obtained for SB 242784 and INH-1 (0.33 and 0.31, respectively) are very close to the fundamental anisotropy of SB 242784 [$\langle r \rangle = 0.34$ (*27*)], which is expected to be identical for INH-1. This cannot be solely explained by the very small fluorescence lifetimes of the inhibitors and must also result from significant immobilization in the bilayer due to the indole moiety anchoring. INH-1 fluorescence anisotropy is slightly lower than SB 242784's, but this divergence can be explained by the differences in fluorescence lifetimes of the two inhibitors.

Regarding the results of the linear dichroism studies, they point to identical orientations of the two inhibitors. Both molecules possess defined preferred orientations around 45° relative to the bilayer normal (45° for SB 242784 and 47° for INH-1), but the SB 242784 orientational distribution function is broader than the corresponding function of INH-1 (Figure 7). This was expected, as the structure of INH-1 is mostly made up of the indole ring double bond conjugated system and does not have freedom of movement around the double bonds. In SB 242784, due to the presence of the piperidine ring connected to the fluorophore by the amide, a larger perturbation in the packing with the lipids is induced, and consequently this packing will not be as tight as with INH-1. This is further supported by the spectral shifts previously described. The population of inhibitors near the surface is more solvated and accordingly is emitting at longer

wavelengths. At variance, the fraction of molecules deeper inside the membrane is emitting more in the blue. This would explain the observed shifts in fluorescence emission maximum in the presence of quenchers at different depths in the bilayer for SB 242784. The tilted configuration of SB 242784, and the resulting poor packing with the bilayer lipids, can be the explanation for the perturbations on lipid mobility induced by the presence of this V-ATPase inhibitor in the bilayer as detected by ESR (*40*).

The orientational probability density function (Figure 7) of SB 242784 has a small contribution near 90°. This contribution is very likely to be spurious and probably results from the data analysis method (*15*), as it seems unlikely that a population of the inhibitors lies parallel to the bilayer surface in view of the other results presented in this study, and bilayer defects that could induce a closer to random orientation of the molecule were absent in the INH-1 samples in the same lipid system. On the other hand, the contribution to the orientational probability density function of SB 242784 for smaller angles relative to the bilayer normal could originate from a fraction of SB 242784 presenting orientations closer to the bilayer normal, due to the presence of the piperidine ring, which, as already mentioned, is expected to prefer the hydrocarbon core of the bilayer and therefore to dislocate the inhibitor toward the bilayer center.

CONCLUSIONS

Summarizing our results, both inhibitors readily aggregate in an aqueous environment and present relatively large partition coefficients to lipid bilayers. It is reasonable to place the fluorophore section of the inhibitors close to the polar/apolar interface of the bilayer, in contact with the headgroup region but still protected from the aqueous environment. The conjugated double bonds are likely to be in contact with the first carbons of the lipid acyl chains, and for the SB 242784 V-ATPase inhibitor the piperidine ring should insert deeper among the acyl chains. The localization of the molecules in bilayers seems to be almost completely dictated by the fluorophore moiety, shared to a large extent by the two molecules. In this way, and assuming that the first step is the inhibitor incorporation in the membrane followed by diffusion to the protein, it would be likely that the site for interaction in the protein would be at a similar position inside the membrane to maximize the diffusional encounters.

The two inhibitors studied here are samples of the entire indole class of V-ATPase inhibitors. SB 242784 exhibits very high inhibitory activities against osteoclastic V-ATPase, with efficient inhibition in nanomolar concentrations, whereas INH-1 is capable of inhibition of the enzyme only in micromolar concentrations (*5*−*7*). According to our results, it can be inferred that this high difference in inhibitory efficiency inside the class of V-ATPase indole inhibitors is essentially due to specific molecular recognition processes with the enzyme inhibition site. The behavior in membranes of the two molecules is very similar, namely, its effective concentration in the membrane, since the partition coefficients do not vary significantly. This strong discrimination by the enzyme reflected on their IC_{50} values (30 μM and 26 nM for INH-1 and SB 242784, respectively) is interesting, considering the close similarity of the two molecules. Experiments are under way to study the interactions of V-ATPase inhibitors with selected transmembrane segments of the enzyme to gain further insight into the protein−inhibitor recognition process.

ACKNOWLEDGMENT

We thank Benedito Cabral for the TD-DFT calculations with SB 242784.

REFERENCES

1. Baron, R., Neff, L., Louvard, D., and Courtoy, P. J. (1986) Cell-mediated extracellular acidification and bone resorption: evidence for a low pH in resorbing lacunae and localization of a 100-kD lysosomal membrane protein at the osteoclast ruffled border, *J. Cell Biol. 101*, 2210−2222.
2. Blair, H. C., Teitelbaum, S. L., Ghiselli, R., and Gluck, S. (1989) Osteoclastic bone resorption by a polarized vacuolar proton pump, *Science 245*, 855−857.
3. Bowman, E. J., Siebers, A., and Altendorf, K. (1988) Bafilomycins: a class of inhibitors of membrane ATPases from microorganisms, animal cells, and plant cells, *Proc. Natl. Acad. Sci. U.S.A. 85*, 7972−7976.
4. Sundquist, K., Lakkakorpi, P., Wallmark, B., and Väänänen, K. (1990) Inhibition of osteoclast proton transport by bafilomycin A1 abolishes bone resorption, *Biochem. Biophys. Res. Commun. 168*, 309−313.
5. Gagliardi, S., Nadler, G., Consolandi, E., Parini, C., Morvan, M., Legave, M. N., Belfiore, P., Zocchetti A., Clarke, G. D., James, I., Nambi, P., Gowen, M., and Farina, C. (1998) 5-(5,6-Dichloro-2-indolyl)-2-methoxy-2,4-pentadienamides: Novel and selective inhibitors of the vacuolar H^+-ATPase of osteoclasts with bone antiresorptive activity, *J. Med. Chem. 41*, 1568−1573.
6. Nadler, G., Morvan, M., Delimoge, I., Belfiore, P., Zocchetti, A., James, I., Zembryki, D., Lee-Rycakzewski, E., Parini, C., Consolandi, E., Gagliardi, S., and Farina, C. (1998) (2*Z*,4*E*)-5-(5,6-Dichoro-2-indolyl)-2-methoxy-*N*-(1,2,2,6,6-pentamethylpiperidin-4-yl)-2,4-pentadienamide, a novel, potent and selective inhibitor of the osteoclast V-ATPase, *Bioorg. Med. Chem. Lett. 8*, 3621−3626.
7. Visentin, L., Dodds, R. A., Valente, M., Misiano, P., Bradbeer, J. N., Oneta, S., Liang, X., Gowen, M., and Farina, C. (2000) A selective inhibitor of the osteoclastic V-H^+-ATPase prevents bone loss in both thyroparathyroidectomized and ovariectomized rats, *J. Clin. Invest. 106*, 309−318.
8. Mattsson, J. P., and Keeling, D. J. (1996) [^{3}H]Bafilomycin as a probe for the transmembrane proton channel of the osteoclast vacuolar H(+)-ATPase, *Biochim. Biophys. Acta 1280*, 98−106.
9. Zhang, J., Feng, Y., and Forgac, M. (1994) Proton conduction and bafilomycin binding by the V_o domain of the coated vesicle V-ATPase, *J. Biol. Chem. 269*, 23518.
10. Crider, B. P., Xie, X. S., and Stone, D. K. (1994) Bafilomycin inhibits proton flow through the H^+ channel of vacuolar proton pumps, *J. Biol. Chem. 269*, 17379−17381.
11. Wang, Y., Inoue, T., and Forgac, M. (2005) Subunit a of the yeast V-ATPase participates in binding of bafilomycin, *J. Biol. Chem. 280*, 40481−40488.
12. Dixon, N., Páli, T., Kee, T. P., and Marsh, D. (2004) Spin labelled V-ATPase inhibitors in lipid membranes, *Biochim. Biophys. Acta 1665*, 177−183.
13. Mayer, L. D., Hope, M. J., and Cullis, P. R. (1986) Vesicles of variable sizes produced by a rapid extrusion procedure, *Biochim. Biophys. Acta 858*, 161−168.
14. McClare, C. (1971) An accurate and convenient organic phosphorus assay, *Anal. Biochem. 39*, 527−530.
15. Castanho, M. A. R. B., Lopes, S., and Fernandes, M. (2003) Using UV-Vis. linear dichroism to study the orientation of molecular probes and biomolecules in lipidic membranes, *Spectroscopy 17*, 377−398.
16. Lakowicz, J. R. (1999) *Principles of Fluorescence Spectroscopy*, 2nd ed., Kluwer Academic/Plenum Publishers, New York.
17. Chen, R., and Bowman, R. L. (1965) Fluorescence polarization: measurements with ultraviolet-polarizing filters in a spectrophotofluorometer, *Science 147*, 729−732.
18. Eaton, D. F. (1988) Reference materials for fluorescence measurement, *Pure Appl. Chem. 60*, 1107−1114.

19. Loura, L. M. S., Fedorov, A., and Prieto, M. (2000) Membrane probe distribution heterogeneity: a resonance energy transfer study, *J. Phys. Chem. B 104*, 6920−6931.
20. Marquardt, D. W. (1963) An algorithm for least squares estimation of non linear parameters, *J. Soc. Ind. Appl. Math. 11*, 431−441.
21. Kooyman, R. P. H., Levine, Y. K., and Van der Meer, B. W. (1981) Measurement of second and fourth rank order parameters by fluorescence polarization experiments in a lipid membrane system, *Chem. Phys. 60*, 317−326.
22. Lopes, S., and Castanho, M. A. R. B. (2002) Revealing the orientation of nystatin and amphotericin B in lipidic multibilayers by UV-Vis linear dichroism, *J. Phys. Chem. B 106*, 7278−7282.
23. Parr, R. G., and Yang, W. (1989) *Density Functional Theory of Atoms and Molecules*, Oxford University Press, Oxford.
24. Becke, A. D. (1993) Density-functional thermochemistry. 3. The role of exact exchange, *J. Chem. Phys. 98*, 5648.
25. Lee, C., Yang, W., and Parr, R. G. (1988) Development of the Colle-Salvetti correlation-energy formula into a functional of the electron density, *Phys. Rev. 37*, 785−789.
26. Hariharan P. C., and Pople, J. A. (1974) Accuracy of AHn, equilibrium geometries by single determinant molecular orbital theory, *Mol. Phys. 27*, 209.
27. Fernandes, F., Loura, L. M. S., Koehorst, R., Hemminga, M., and Prieto, M. (2004) Interaction of the indole class of V-ATPase inhibitors with lipid bilayers, *Biophys. J. 88*, 240a.
28. Santos, N. C., Prieto, M., and Castanho, M. A. R. B. (2003) Quantifying molecular partition into model systems of biomembranes: an emphasis on optical spectroscopic methods, *Biochim. Biophys. Acta 1612*, 123−135.
29. Tristram-Nagle, S., Petrache, H. I., and Nagle, J. F. (1998) Structure and interactions of fully hydrated dioleoylphosphatidylcholine bilayers, *75*, 917−925.
30. Chattopadhyay, A., and London, E. (1987) Parallax method for direct measurement of membrane penetration depth utilizing fluorescence quenching by spin-labeled phospholipids, *Biochemistry 26*, 39−45.
31. Abrams, F. S., and London, E. (1992) Calibration of the parallax fluorescence quenching method for determination of membrane penetration depth: refinement and comparison of quenching by spin-labeled and brominated lipids, *Biochemistry 31*, 5312−5322.
32. Runnels, L. W., and Scarlata, S. F. (1995) Theory and application of fluorescence homotransfer to melittin oligomerization, *Biophys. J. 69*, 1569−1583.
33. Berberan-Santos, M. N., and Prieto, M. J. E. (1987) Energy transfer in spherical geometry. Application to micelles, *J. Chem. Soc., Faraday Trans. 83*, 1391−1409.
34. de Almeida, R. F. M., Loura, L. M. S., Prieto, M., Watts, A., Fedorov, A., and Barrantes, F. J. (2004) Cholesterol modulates the organization of the M4 transmembrane domain of the muscle nicotinic acetylcholine receptor, *Biophys. J. 86*, 2261−2272.
35. Koehorst, R. B. M., Spruijt, R. B., Vergeldt, F. J., and Hemminga, M. A. (2004) Lipid bilayer topology of the transmembrane alfa-helix of M13 major coat protein and bilayer polarity profile by site-directed fluorescence spectroscopy, *Biophys. J. 87*, 1445−1455.
36. White, S. H., and Wimley, W. C. (1998) Hydrophobic interactions of peptides with membrane interfaces, *Biochim. Biophys. Acta 1376*, 339−352.
37. Contreras, L. M., de Almeida, R. F. M., Villalaín, J., Fedorov, A., and Prieto, M. (2001) Interaction of -melanocyte stimulating hormone with binary phospholipid membranes: structural changes and relevance of phase behaviour, *Biophys. J. 80*, 2273−2283.
38. Yau, W., Wimley, W. C., Gawrisch, K., and White, S. H. (1998) The Preference of tryptophan for membrane interfaces, *Biochemistry 37*, 14713−14718.
39. de Planque, M. R. R., Kruijtzer, J. A. W., Liskamp, R. M. J., Marsh, D., Greathouse, D. V., Koeppe II, de Kruijff, B., and Killian, J. A. (1999) Different membrane anchoring positions of tryptophans and lysine in synthetic transmembrane alpha-helical peptides, *J. Biol. Chem. 274*, 20839−20846.
40. Páli, T., Dixon, N., Kee, T. P., and Marsh, D. (2004) Incorporation of the V-ATPase inhibitors concanamycin and indole pentadiene in lipid membranes. Spin-label EPR studies, *Biochim. Biophys. Acta 1663*, 14−18.

BI0522753